Bioinspired wingtip devices: a pathway to improve aerodynamic performance during low Reynolds number flight

Bioinspiration & Biomimetics

PAPER

Bioinspired wingtip devices: a pathway to improve aerodynamic performance during low Reynolds number flight

RECEIVED
19 March 2017

REVISED
11 January 2018

ACCEPTED FOR PUBLICATION
1 February 2018

PUBLISHED
20 March 2018

Michael Lynch, Boris Mandadzhiev and Aimy Wissa

Department of Mechanical Science and Engineering, University of Illinois at Urbana-Champaign, 1206 W Green St., Urbana, IL 61801, United States of America

E-mail: awissa@illinois.edu

Keywords: Avian-inspired flight, wingtip devices, low Reynolds number, multiple winglets, segmented wingtip, slotted wing tips

Abstract

Birds are highly capable and maneuverable fliers, traits not currently shared with current small unmanned aerial vehicles. They are able to achieve these flight capabilities by adapting the shape of their wings during flight in a variety of complex manners. One feature of bird wings, the primary feathers, separate to form wingtip gaps at the distal end of the wing. This paper presents bio-inspired wingtip devices with varying wingtip gap sizes, defined as the chordwise distance between wingtip devices, for operation in low Reynolds number conditions of Re = 100 000, where many bird species operate. Lift and drag data was measured for planar and nonplanar wingtip devices with the total wingtip gap size ranging from 0% to 40% of the wing's mean chord. For a planar wing with a gap size of 20%, the mean coefficient of lift in the pre-stall region is increased by 7.25%, and the maximum coefficient of lift is increased by 5.6% compared to a configuration with no gaps. The nonplanar wingtip device was shown to reduce the induced drag. The effect of wingtip gap sizes is shown to be independent of the planarity/nonplanarity of the wingtip device, thereby allowing designers to decouple the wingtip parameters to tune the desired lift and drag produced.

Nomenclature

α_b	Base wing angle of attack
α_t	Wingtip angle of attack
b	Total wingspan
b_b	Base wing span
b_t	Wingtip span
c_b	Base wing chord
c_t	Wingtip chord
AR	Aspect ratio
Re	Reynolds number
C_{Di}	Induced drag coefficient
C_{Dpar}	Parasitic drag coefficient
C_D	Drag coefficient
C_L	Lift coefficient
C_{Lmax}	Maximum lift coefficient
γ	Total wingtip gap size %
e	Oswald's efficiency factor
e_{wl}	Oswald's efficiency factor for winglets
V_∞	Freestream velocity
ρ_∞	Air density
S	Wing planform area
h	Winglet height
k_{wl}	Winglet induced drag penalty factor

1. Introduction

1.1. Motivation and goals

Birds are highly capable and maneuverable fliers, with the ability to fly at both high and low speeds in a variety of flight conditions. They engage in a multitude of complex flight maneuvers, such as takeoff, landing, gliding, perching, diving, and more. Mission adaptability is enabled through changing the shape of their wings and their wing-beat gaits during flight in a variety of complex ways [1]. These abilities are not shared with today's small unmanned aerial vehicles (UAVs) [2].

Unlike birds, current small UAVs struggle to fly in gusty and turbulent conditions and are mostly relegated to fair weather flight [2]. Mohamed *et al* assessed a variety of factors that prevent small UAVs from having stable flight characteristics including: low mass, power limitations, slow and low flight, and low Reynolds number conditions.

Among the factors affecting UAV flight, the low Reynolds number operating condition is perhaps the most significant obstacle to overcome. Airfoil performance diminishes at lower Reynolds numbers,

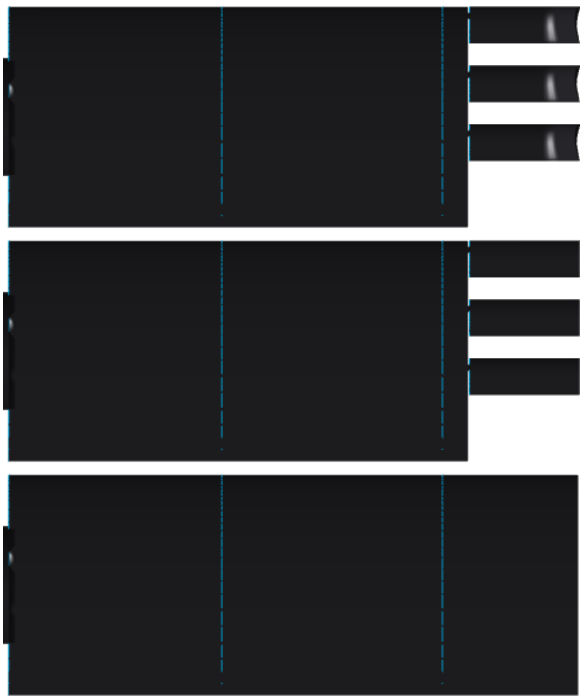

Figure 1. Top: nonplanar wingtip configuration with $\gamma = 20\%$. Middle: planar wingtip configuration with $\gamma = 20\%$. Bottom: wingtip extension.

decreasing the coefficient of lift and increasing the coefficient of drag [3]. In examining the efficiency of airplane airfoils in comparison with bird wings, Withers [4] demonstrates that bird wings perform similarly to conventional airfoils at low Reynolds numbers. Despite this, birds are still able to outmaneuver and outperform UAVs, especially in high angle of attack maneuvers such as perching [5]. This demonstrates the need for a shift in approach away from optimizing fixed airfoil designs for low Reynolds numbers, and instead, looking to birds for inspiration on adaptive wing structures.

When examining birds' wings, there are many notable feather systems used by birds to improve mission adapatbility. These include the primaries, the secondaries, the coverts, and the alula feathers [6]. Each category of feather has a different function relating to flight. In particular, the primary feathers have been shown to reduce the induced drag [7]. The birds' wingtips can provide insight on how to improve the wingtip design of small UAVs. The objective of this paper is to understand the effect of wing gaps (figure 1) on the lift and drag production at low Reynolds number conditions. The effects of wingtip planarity (figure 2) at different gap sizes will also be investigated.

1.2. Background and previous works

When categorizing bird wing planforms, Savile categorize bird wings into four broad shapes as seen in figure 3: soaring wings (Albatross), high speed wings (Falcon), elliptically shaped wings (Crow), and high lift wings (Eagle) [8].

Small UAVs fly in environments that are relatively close to ground level, filled with obstacles such as trees and buildings, and characterized by high levels of turbulence [10]. Among the previously mentioned categories, two types of bird wing shapes operate in similar conditions: elliptically shaped wings and high lift wings. Elliptically shaped wings, as seen on birds such as crows, allow for high degrees of maneuverability [8]. High lift wings, as seen on eagles and hawks, are used by birds of prey that need to carry large payloads. Wings of high lift birds have greater agility than soaring wings or high speed wings. In particular, high lift wings have similar requirements as wings used by modern UAVs due to the payload demands of UAVs, and as such, they will be the focus of this study.

When looking at various wing structures present on high lift wings, one notable feature is the presence of wingtip gaps as shown in figure 4. These gaps are created due to primary feather emargination.

Some bird feathers are not shaped like ellipses, but instead have a tapered region, and the emargination of the bird feathers is the point at which the taper begins. As can be seen in figure 5, the emargination is where the feather tapers at the leading edge, and the notch is where the feather tapers at the trailing edge. While it varies for different species, usually the first 5–6 primary feathers have significant emargination, as seen in figure 6. This is because these are the feathers that form the leading edge of the wing while the remaining feathers form the trailing edge.

To understand the effect wingtip gaps have on bird flight characteristics, Tucker conducted wind tunnel experiments on a Harris Hawk wing [7]. Tucker

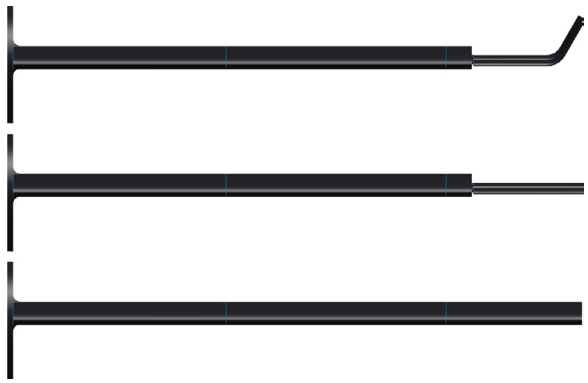

Figure 2. Top: nonplanar wingtip configuration. Middle: planar wingtip configuration. Bottom: wingtip extension.

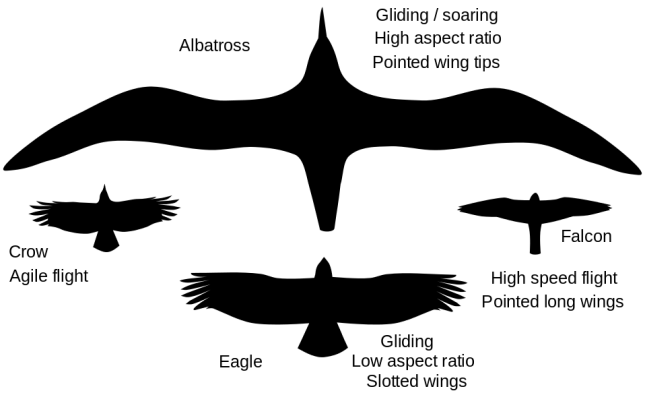

Figure 3. Wing shapes: soaring wings (albatross), high speed wings (falcon), high lift wings (eagle), and elliptical wings (crow). Bird flight silhouettes by Shyamal (own work) (CC BY-SA 2.5 (http://creativecommons.org/licenses/by-sa/2.5)), via Wikimedia Commons [9].

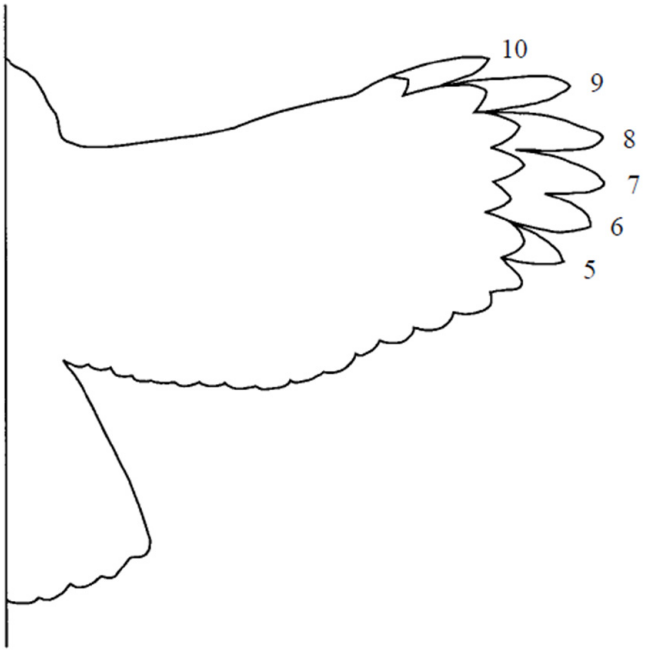

Figure 4. Wingtip gaps of a Harris hawk. Reproduced/adapted with permission from the Journal of Experimental Biology (www.jeb.biologists.org) [7].

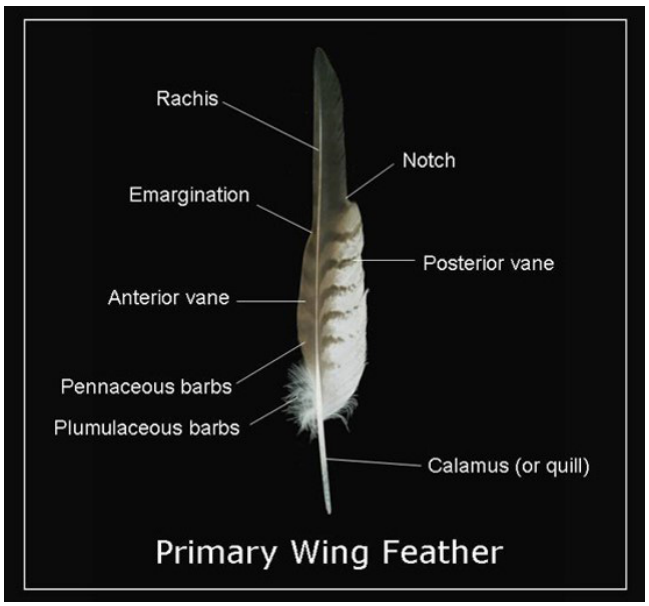

Figure 5. Bird feather emargination and notch, forming the wingtip gaps. Adapted from [11].

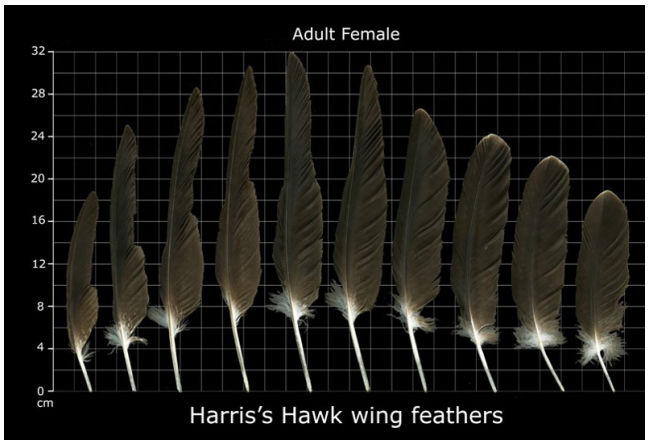

Figure 6. Primary feathers of an adult Harris hawk. Adapted from [11].

found that wing gaps reduced the induced drag of a Harris Hawk wing by acting as nonplanar winglets and spreading the vorticity both horizontally and vertically. Induced drag is the component of drag generated due to the lifting force. The reduction of induced drag is especially important in the design of small UAVs, because, at low Reynolds number and low flight speeds, induced drag forms a large component of the total drag on an aircraft [12].

Studies of nonplanar structures, such as winglets, were first rigorously conducted by Whitcomb. Whitcomb [13] showed that the induced drag on airplanes can be reduced by 20% under certain conditions with the incorporation of properly designed winglets. This is a significant benefit since induced drag can make up 40% of an airplane's drag under cruise conditions and up to 80–90% of drag under takeoff conditions [14].

Despite all of these developments, according to the authors' knowledge, there have been very few and limited instances of research conducted on winglets for low Reynolds number conditions where small UAVs usually perform. Most work done on wingtip devices, such as the work done by Kroo [12], La Roche and Palffy [15], and Fluckand Crawford [16] have all focused on vehicles which operate at higher Reynolds numbers ($Re \geqslant 1.0 \times 10^6$).

Among the work that considers low Reynolds operation, the most relevant are the works done by Cerón-Muñoz and Catalono [17], Guerrero *et al* [18], and Smith *et al* [19]. Smith *et al* examined the lift to drag ratio on a multi-winglet configuration in low Reynolds number conditions ranging from 161 000 to 300 000 and concluded that the ratio was improved by 15–30% for a configuration where the winglet dihedral angle is varied as compared with a configuration angle with constant dihedral angle [19]. However, despite this overall improvement in the lift to drag ratio, while the actual lift force increased, the overall drag force also increased. Many questions remain about how exactly

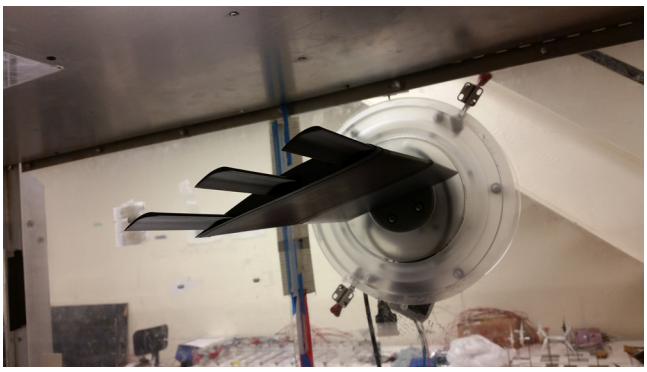

Figure 7. Experimental setup with $\gamma = 40\%$ and the $(0, 0, 0)$ configuration for α_t.

wingtip devices affect induced drag, especially at low Reynolds numbers.

The goal of this paper is to develop a more complete understanding of how wingtip gaps and planarity affect the aerodynamic performance of small UAVs at low Reynolds numbers. In the following sections, a bio-inspired wingtip device design with varying gap sizes, wingtip angles of attack, and planarity, is presented. The results of wind tunnel tests conducted on various configurations of wingtip devices run at varying Reynolds numbers are shown. The final section includes a discussion on actuation of such devices along with proposed future work.

2. Methods

2.1. Experimental setup

Wind tunnel tests were conducted in an open-loop, constant pressure wind tunnel with a cross section of 90 cm by 45 cm at the University of Illinois Urbana-Champaign. The wind tunnel had four equal length sections. The first section was chosen for testing to minimize the boundary layer thickness and least turbulence (0.1%). The tests were run at $\mathrm{Re} = 1.0 \times 10^5$ where the Reynolds number characteristic length was the base wing chord length, c_b. The flow velocity was calibrated to 10.1 m s^{-1} by using a static-pitot tube attached to a differential pressure sensor.

The wing system, which consists of the base wing and the wingtip devices, was mounted to a custom-made housing system in the sidewall of the wind tunnel (figure 7). The housing system contained a Velmex B48 rotary table which was used for precision control of the base wing angle of attack, α_b. A stepper motor and micro stepper driver were used to actuate the Velmex B48 rotary table such that α_b could be controlled with a precision of 0.0125°.

Attached to the rotary table was an ATI Gamma 6-axis force/torque transducer, used to collect the lift and drag forces on the wing. Because the force/torque transducer was rotated with the wing, a rotation matrix with mass compensation was used to obtain the netl lift and drag forces at a given α_b. The force/torque transducer had a range of 0–32 N, a resolution of 1/160 N, and fullscale measurement uncertainties of 0.75% in the X and Y axes, which correspond with the lift and drag force directions, respectively.

For each test, force data was collected at 1000 Hz for 10 s while at steady state. The data was averaged to determine the lift and drag forces for a specific test configuration. Each test configuration was tested three times to compensate for low Reynolds number unsteadiness, and the mean of the three values is the reported force.

2.2. Wing and wingtip parameters

In this experiment, the wing and wingtip device geometry were modeled after the Harris Hawk. The base wing is a rectangular wing with an SD7032 airfoil, an airfoil designed to produce high lift in low Reynolds number conditions ranging from $\mathrm{Re} = 8.0 \times 10^4$ to $\mathrm{Re} = 3.0 \times 10^5$ [20]. The base wing chord length, c_b, is 150 mm and the wing has a semi-span, $b_b/2$ of 312.5 mm.

The primary feathers of a Harris Hawk were measured from digital images obtained from the Feather Atlas [11]. These were used as a basis for the geometry of the wingtip devices, modeled in this experiment as S1091 airfoils with 10% thickness. Based on the geometry of the Harris Hawk primary feathers, the chord length of one wingtip, c_t, was found to be 16.7% of the c_b, or 25 mm and the wingtip span, b_t, was found to be 12% of the base wingspan, b_b, or 75 mm.

A nonplanar wingtip was designed such that b_t and c_t were the same as for the planar wingtips. The nonplanar wingtip height, h, was set at 7.5% of the semi-span of the wing-winglet system as described in equation (1). The wingtip cant angle was set to 60°, and the winglet bend radius was set to 50% of h. Figure 8 shows the nonplanar geometry

$$h = \left(\frac{b_b}{2} + b_t\right) 0.075. \tag{1}$$

A planar configuration is defined as the base wing with three planar wingtips, while a nonplanar configuration is defined as the base wing with three nonplanar wingtips. In addition to the planar and nonplanar

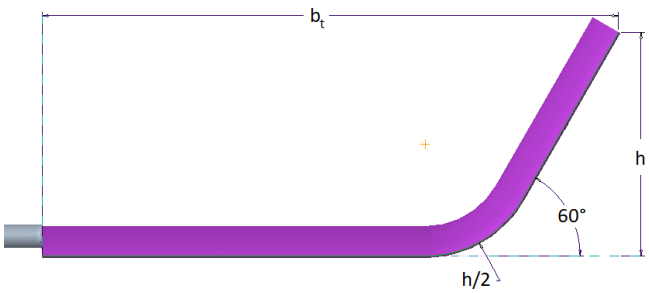

Figure 8. Nonplanar wingtip geometry parameters where h is the wingtip height and b_t is the span of the wing tip.

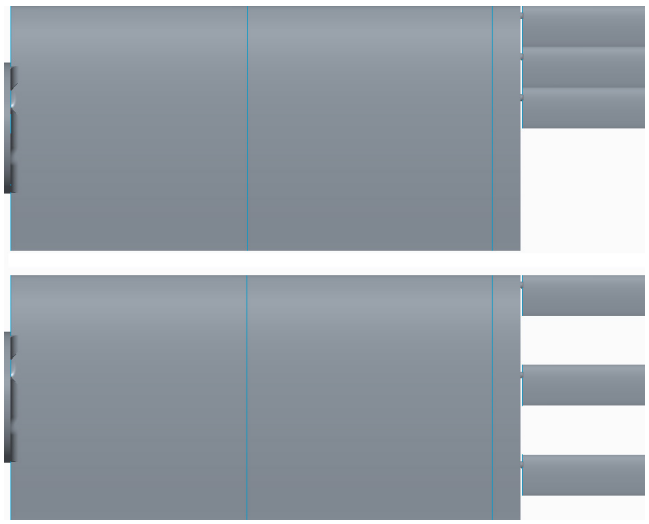

Figure 9. Top: wing-wingtip configuration with $\gamma = 0\%$. Bottom: wing-wingtip configuration with $\gamma = 40\%$.

configurations, a baseline wingtip extension was tested. The baseline test was designed such that the base wingspan was increased to maintain the overall span of the wing-wingtip system.

The overall aspect ratio of the wing-wingtips system is 5.72, which falls in the range of 4–6 for the AR of high lift wings in birds [8]. The wing-wingtip extension system has an aspect ratio of 5.17 since the wingtip extension had the same span, but a larger planform area, S.

The total wingtip gap size percentage, γ, is defined as total gap spacing between all of the feathers/wingtip devices divided by the base wing chord length. For a Harris hawk with its wings fully spread, the emargination of the feathers leads to gaps between the feathers that are nonuniform in length. Using image analysis, the average chordwise distance of the gaps is measured to be between 5%–8% of the mean wing chord, c_b, between individual feathers. When summed together, this leads to a γ value of 31% for the Harris Hawk.

2.3. Test configurations

Several wing-wingtip system configurations were tested. The planar and nonplanar wingtips were tested with varying gap sizes, γ, of 0%, 20%, 30%, and 40%. Gap sizes $\gamma = 0\%$ and $\gamma = 40\%$ are shown in figure 9. For each configuration, the base wing angle of attack, α_b was varied from 6° to 21°. This allowed for detailed measurements of aerodynamic forces in the pre-stall and post-stall regions.

Table 1. Sets of tested wingtip angles of attack, α_t.

Leading α_t	Secondary α_t	Trailing α_t
0°	0°	0°
−10°	−10°	−10°
−10°	−5°	0°
−10°	0°	10°

In flight, the wingtips of birds are offset at various angles of attack due to the interaction with the air. Graham explains that the wingtips twist forward, bend upward, and bend forward as a result of the wingtips yielding to the reaction of the displaced air. The wingtips, offset at various angles of attack, deflects the air such that the direction of the air stream is gradually changed [21]. To account for the effect of the wingtip angles of attack, the wingtips were set at an angle of attack, α_t, relative to the base wing in 4 different configurations as shown in table 1. The shaft attaching the wingtips to the base wing were located at the wingtip segment quarter chord ($\frac{c_t}{4}$). The hole locations for the wingtip shafts were located along the camber line of the base wing.

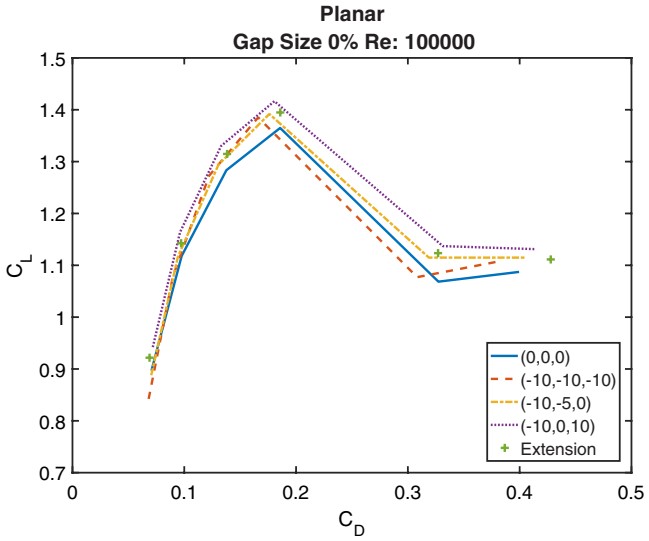

Figure 10. C_L versus C_D for the planar configuration comparing the effect of varying wingtip angle of attack, α_t, at $\gamma = 0\%$.

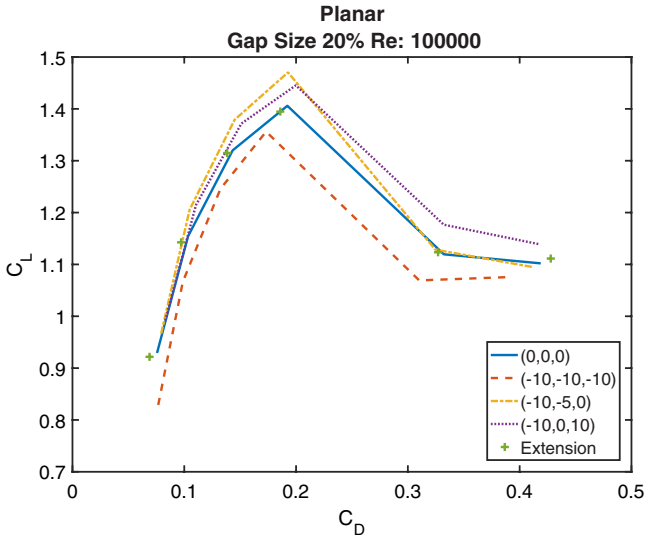

Figure 11. C_L versus C_D for the planar configuration comparing the effect of varying wingtip angle of attack, α_t, at $\gamma = 20\%$.

3. Results and discussion

The non-dimensional lift and drag coefficient were calculated from the force transducer data and based on the geometric and test parameters in accordance with equations (2) and (3). In these equations, the area, S, refers to the planform area of the wing-winglet or wing-extension system

$$C_L = \frac{L}{\frac{1}{2}\rho_\infty V_\infty^2 S} \quad (2)$$

$$C_D = \frac{D}{\frac{1}{2}\rho_\infty V_\infty^2 S}. \quad (3)$$

3.1. Effect of wingtip angles of attack

Figures 10–13 demonstrate the effect of varying sets of α_t, as defined in table 1, on C_L versus C_D in the planar configuration for each of the tested gap sizes, γ.

In figure 10, the planar configuration with a gap size of $\gamma = 0\%$ shows that the $(0, 0, 0)$ configuration of α_t produces the least amount of lift and the most drag in the pre-stall region of α_b, 6°–15°. This configuration produces a 2% lower C_{Lmax} than the wingtip extension. The $(-10, 0, 10)$ set of α_t angles produces the highest overall $C_{Lmax} = 1.416$, 1.6% higher than the wingtip extension and 3.7% higher than the $(0, 0, 0)$ configuration while incurring a relatively low drag penalty compared to all other configurations.

However, in figure 11 which compares α_t sets for $\gamma = 20\%$, the $(-10, -10, -10)$ configuration produces the least amount of lift and incurs the highest drag penalty, the $(0, 0, 0)$ configuration and the wingtip extension's performance become very similar, and the $(-10, -5, 0)$ configuration produces the greatest C_{Lmax} in the pre-stall region. The C_{Lmax} value of the $(-10, -5, 0)$ configuration is 5.45% higher than the C_{Lmax} of the wingtip extension and 4.55% higher than

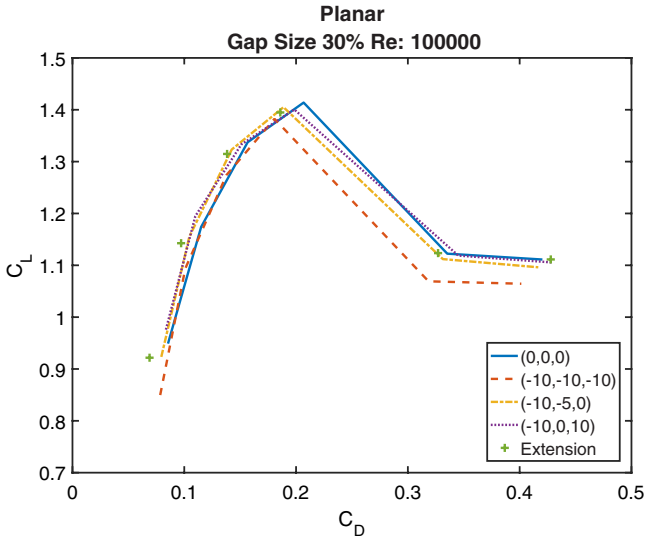

Figure 12. C_L versus C_D for the planar configuration comparing the effect of varying wingtip angle of attack, α_t, at $\gamma = 30\%$.

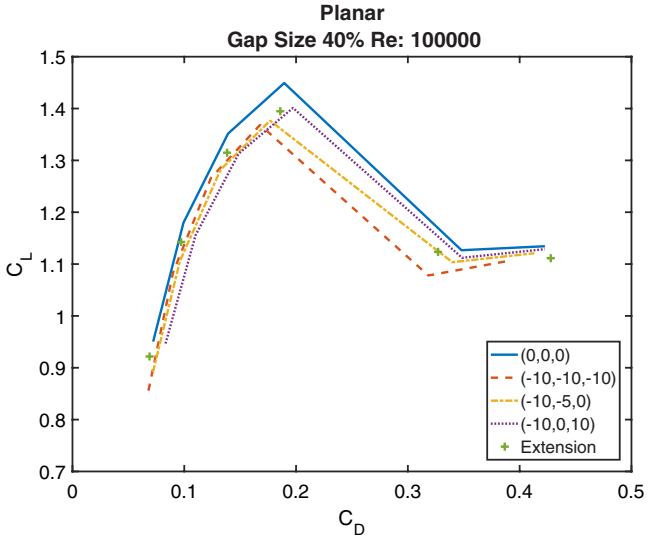

Figure 13. C_L versus C_D for the planar configuration comparing the effect of varying wingtip angle of attack, α_t, at $\gamma = 40\%$.

the (0, 0, 0) configuration. This configuration has the highest overall C_{Lmax} of any configuration tested. In comparison with the next best configuration at this gap size, the $(-10, 0, 10)$ configuration, the $(-10, -5, 0)$ configuration has a 1.7% higher C_{Lmax} and 3.5% lower C_D at C_{Lmax} resulting in an L/D ratio that is 5.42% higher for the $(-10, -5, 0)$ configuration than for the $(-10, 0, 10)$ configuration.

In figure 12, the performance of all wingtip systems becomes very similar in the pre-stall region. The wingtip extension produces the least amount of drag of any configuration at lower values of $C_L \leqslant 1.3$, indicating that all other tested sets of α_t produced less lift and more drag at this gap size. The (0, 0, 0) configuration is able to produce the largest C_{Lmax}, but does so while producing 11.1% more C_D than the wingtip extension, resulting in a L/D ratio 8.7% lower than for the wingtip extension at C_{Lmax}.

Figure 13 continues many of the trends shown in figure 12 with most sets of α_t producing more drag and less lift than the wingtip extension. However, the one exception to this trend is that the (0, 0, 0) configuration of α_t improves significantly in lift generation, producing a C_{Lmax} value that is 3.94% higher than C_{Lmax} for the wingtip extension. Unlike in figure 12, the (0, 0, 0) configuration in figure 13 has an L/D ratio 2.13% higher than the L/D ratio of the wingtip extension.

Based on the findings above, it is clear that the performance of the wing-wingtip system depends heavily on the wingtip configuration, with many configurations being detrimental to overall performance. Similar results were also found in Fluck and Crawford's work when performing numerical simulations of wingtip twist, a parameter similar to wingtip angles of attack, at $\mathrm{Re} = 1.3 \times 10^6$ [16].

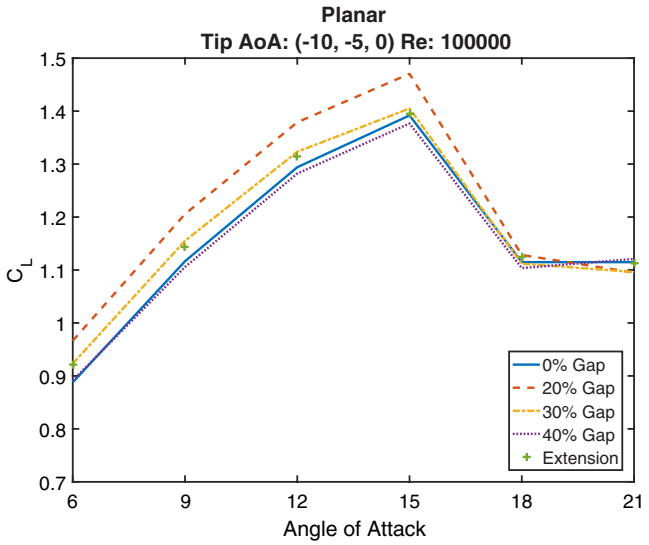

Figure 14. C_L versus α_b for the planar configuration demonstrating the effect of gap size. Varying γ has a large effect on C_L, and choosing $\gamma = 20\%$ provides the greatest increase in C_L across all α_b tested in the pre-stall region.

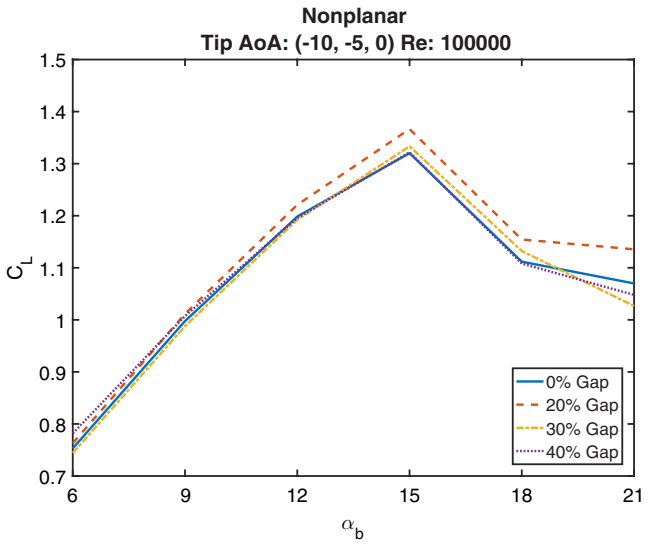

Figure 15. C_L versus α_b for the nonplanar configuration demonstrating the effect of gap size. Changing γ has a reduced effect on C_L, though $\gamma = 20\%$ still provides the greatest benefit to C_L and particularly to C_{Lmax}.

From these results, it is clear that the optimal wingtip configuration changes depending on gap size and desired performance specification ranging from maximizing lift to maximizing the L/D ratio. For this experiment, the remainder of the analysis will focus on the $(-10, -5, 0)$ configuration for α_t since this configuration is the one that produces the greatest C_{Lmax} of any configuration in the pre-stall region of $6^\circ \leqslant \alpha_b \leqslant 15^\circ$.

3.2. Effect of gaps

In analyzing the effect of gaps, both figures 14 and 15 show that there is an improvement in C_L and especially in C_{Lmax}, when $\gamma = 20\%$, over the baseline case of $\gamma = 0\%$ as well as the wingtip extension. For the planar condition, a γ value corresponding to 20% shows a 5.60% improvement in C_{Lmax} over the $\gamma = 0\%$ case and a 5.45% improvement over the wingtip extension. Over the entire range of C_L in the tested pre-stall region, the mean C_L for $\gamma = 20\%$ is 7.25% higher than when $\gamma = 0\%$ and 5.18% higher as compared with the wingtip extension. For the nonplanar configuration, at $\gamma = 20\%$, C_{Lmax} increases by 3.48% and the overall C_L curve is 2.04% higher than for when $\gamma = 0\%$ in the pre-stall region.

However, when γ is increased beyond 20%, there is a reduction in the C_L curves. In the planar case, the reduction is gradual with $\gamma = 30\%$ still having a higher C_{Lmax} than either the wingtip extension or the $\gamma = 0\%$ case. However, once $\gamma = 40\%$, C_{Lmax} is lower than all other cases. For the nonplanar case, shown in figure 15, an increase in gap size to 30% or 40% corresponds with a reduction in C_L across all α_b, and the C_L curves to become indistinguishable.

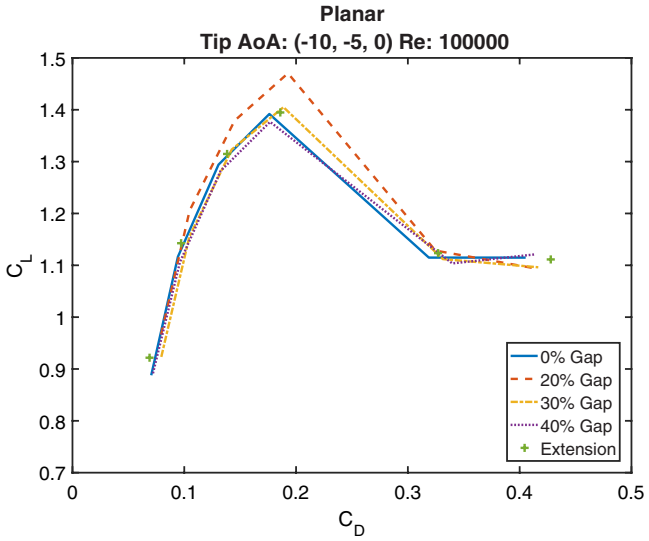

Figure 16. C_L versus C_D for the planar configuration demonstrating the effect of gap size. $\gamma = 20\%$ produces the greatest lift while incurring small drag penalties for the wing-wingtip system.

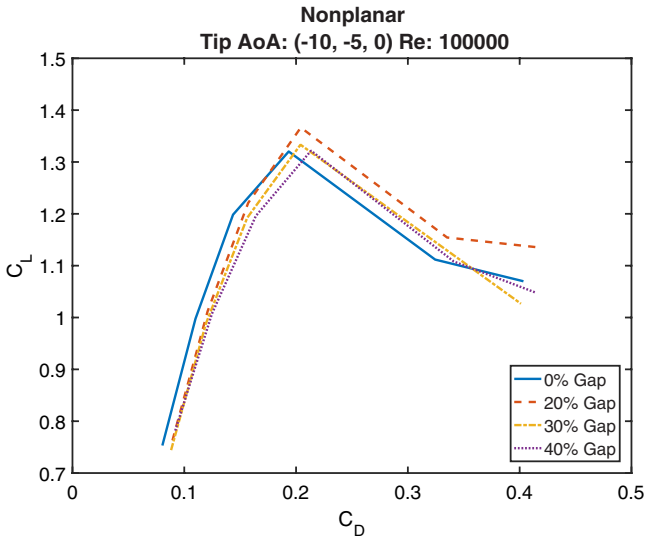

Figure 17. C_L versus C_D for the nonplanar configuration demonstrating the effect of gap size. The presence of wingtip gaps leads to a right shift in the C_L versus C_D curves, leading to a drag penalty for having gaps in the nonplanar configuration.

The general trends in figures 14 and 15 show that the wingtip gaps play a small role in affecting C_L for the nonplanar configuration as compared with the effects on C_L in the planar configuration. This suggests that the drag component due to lift, the induced drag, is relatively unaffected in the nonplanar configuration by wingtip gap sizes, a result which is in agreement with Munk's Stagger Theorem which states that, in a multiplane lifting system, the total induced drag is unaltered if any of the lifting elements are moved in the streamwise direction provided that the lift distribution remains unchanged.

Figures 16 and 17 shows the coefficient of lift plotted against the coefficient of drag for both the planar and nonplanar configurations at various gap sizes and $\alpha_t = (-10, -5, 0)$. The C_L versus C_D curves shown in figure 16 demonstrates that, when $\gamma = 20\%$, the wingtip system is producing the greatest C_L for a given C_D, especially at higher values of C_L. For this configuration, the wingtips generate a larger C_L all while either maintaining C_D, or, in some cases, reducing C_D for a given C_L. In particular, C_{Lmax} is significantly increased for $\gamma = 20\%$ as compared with all other planar configurations while suffering a very minimal C_D increase. Figure 16 also shows that when γ is increased beyond 20%, there is a detrimental effect to C_{Lmax}. In figure 17, the benefits of using a gap size of 20% is reduced. Figure 17 shows a right shift in all of the C_L versus C_D curves for when $\gamma > 0\%$, signifying that for the nonplanar case, there is an increase in drag suffered when gaps are present.

$\gamma = 20\%$ shows the greatest improvement in C_L. These results are consistent in both the planar and nonplanar wingtip cases. Thus, the effects of wingtip

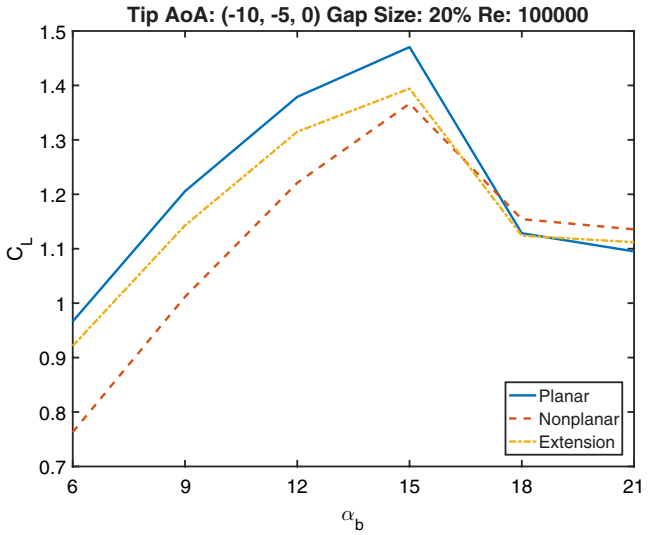

Figure 18. C_L versus α_b demonstrating the effect of planarity. The nonplanar configuration produces significantly less lift than both the wingtip extension and the planar configuration.

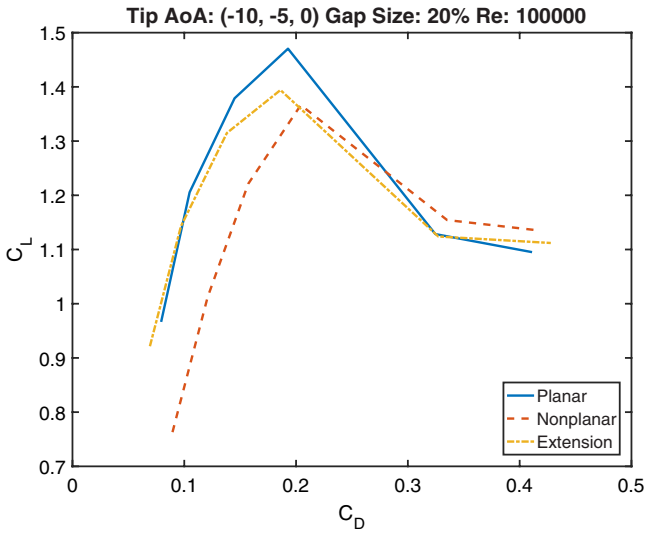

Figure 19. C_L versus C_D demonstrating the effect of planarity. The nonplanar configuration suffers a large drag penalty as compared with the planar configuration and the wingtip extension.

gaps can be decoupled from the planarity of the wingtip geometry.

The effects of planarity can be more clearly seen in figures 18 and 19. Figure 18 shows a plot of C_L over a sweep of α_b for the wingtip extension, planar, and nonplanar configurations where $\gamma = 20\%$ and the $(-10, -5, 0)$ configuration of α_t was used. The nonplanar configuration generated less lift than both the planar configuration and the wingtip extension in the pre-stall region. C_{Lmax} was reduced by 7.07% and the average reduction in C_L across the pre-stall region was 13.92% as compared with the planar configuration. When the nonplanar configuration was compared with the wingtip extension, C_{Lmax} was reduced by only 2.01% while C_L was reduced by 9.44%.

Figure 19 plots C_L against C_D for the wingtip extension, planar, and nonplanar configurations where $\gamma = 20\%$ and α_t corresponded with the $(-10, -5, 0)$ configuration. This graph shows that the nonplanar wingtip devices, in the configurations tested, do not improve C_L for a given C_D, but instead cause a right shift in the C_L versus C_D curve.

3.3. Induced drag

To understand the effects of the wingtip devices on drag, drag must first be broken down into components of induced drag and parasitic drag as shown in equation (4). Other components of drag, such as wave drag, can be ignored due to the low Reynolds number [22]

$$C_D = C_{Dpar} + C_{Di}. \quad (4)$$

Parasitic drag encompasses all aspects of drag not directly associated with lift production. Some components of parasitic drag are profile drag, which is defined as the total of the skin friction drag and form

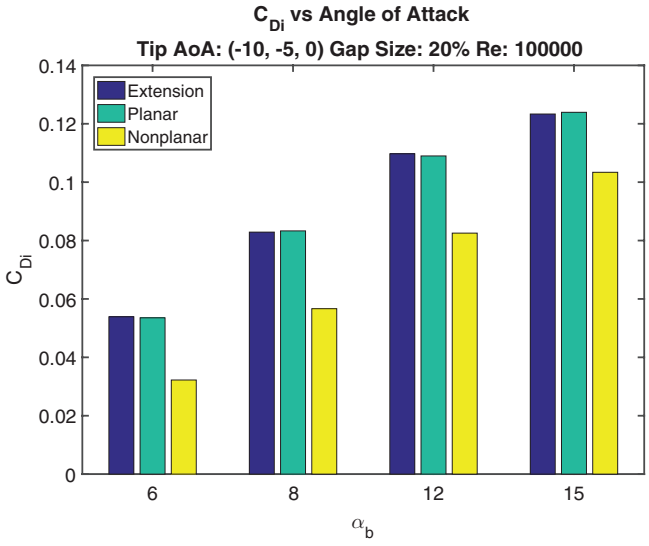

Figure 20. C_{Di} versus α_b for planar and nonplanar configurations for pre-stall angles of attack showing a reduction in induced drag when switching to a nonplanar configuration.

drag for a two-dimensional airfoil section, and interference drag. Skin friction drag is the resulting drag from viscous shearing stresses over the wetted surface of the airfoil. Form drag, sometimes referred to as pressure drag, is defined as the drag resulting from the integrated effect of the static pressure acting normal to its surface, resolved in the drag direction. Interference drag is the increment of drag resulting from two bodies in close proximity to each other such as a wing-fuselage system or, in this case, the wing-winglet system [22].

In contrast to these forms of drag, induced drag is the drag due to lift that results from the generation of trailing vortices [22] and is defined by the empirically derived relationship in (5)

$$C_{Di} = \frac{C_L^2}{\pi AR e}. \tag{5}$$

To calculate C_{Di}, the Oswald's efficiency factor, e, was approximated from figure 4.21 in [22] for the planar configuration. For the nonplanar configuration, modifications to the Oswald's efficiency factor had to be made in accordance with equation (6) derived in [23]

$$C_{Di} = \frac{C_L^2}{\pi AR e_{wl}}. \tag{6}$$

The new Oswald's efficiency factor, e_{wl}, takes into account the geometry of the winglets. The value can be calculated from equation (7)

$$e_{wl} = \left(1 + \frac{2}{k_{wl}}\frac{h}{b}\right)^2 e. \tag{7}$$

In this equation, h is the height of the winglets and b is the total wingspan. This equation tends to overestimate the benefits of winglets, and Niţă and Scholz [23] proposed the addition of a penalty factor, k_{wl} which took into account the effectiveness of a winglet. If the additional height of a winglet were to work identically to a span increase, then $k_{wl} = 1$. Using data from Kroo's work, Niţă and Scholz estimated $k_{wl} = 2.13$ for a winglet configuration similar to the one used in this experiment [14, 23].

It is important to note that this method of calculating the induced drag is an indirect method and is inherently less accurate than a wake pressure study or numerical methods. However, the method used here is still able to determine relative trends in induced drag when comparing different configurations of the wing-winglet system. Future experiments will take advantage of wake pressure methods or numerical methods to obtain more accurate and absolute values for induced drag.

Figure 20 presents the calculated values of C_{Di} for the $(-10, -5, 0)$ configuration of α_t with $\gamma = 20\%$ for the wingtip extension, planar, and nonplanar configurations. This graph shows that, in the pre-stall region, the induced drag is reduced by a significant amount, ranging from 17% to 40%, by switching from the planar to the nonplanar configuration.

Figure 21 shows the calculated values of C_{Dpar} for the $(-10, -5, 0)$ configuration with $\gamma = 20\%$ in both the planar and nonplanar configurations. This graph demonstrates that, by switching to the nonplanar configuration, there is a significant C_{Dpar} penalty.

To understand the context of figures 20 and 21, it is important to understand the design considerations for winglets. One of the major goals of winglet design is often to optimize the winglet geometry such that a maximum reduction in C_{Di} and minimum increase in C_{Dpar} can be achieved, thereby resulting in the lowest possible C_D. The winglets used in this experiment were able to demonstrate a significant reduction in C_{Di} as shown in figure 20, however, this was coupled with an even larger increase in C_{Dpar}. Future experiments using wake measurements or numerical methods can more accurately determine the effects on C_{Di} and C_{Dpar},

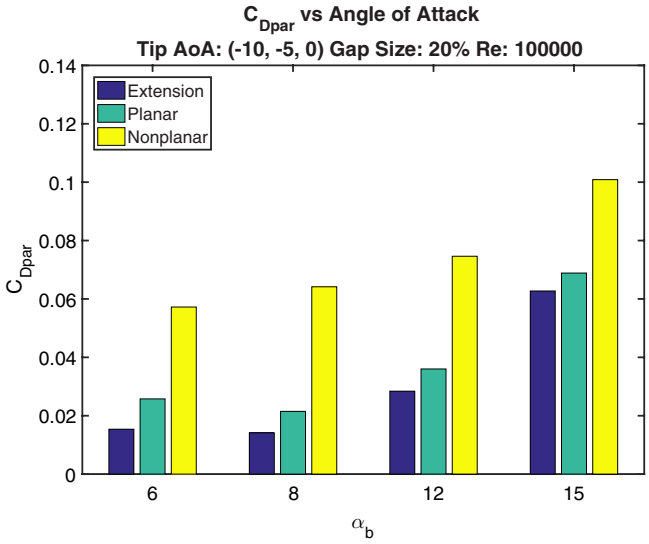

Figure 21. C_{Dpar} versus α_b for planar and nonplanar configurations for pre-stall angles of attack showing an increase in parasitic drag when switching to a nonplanar configuration.

allowing for fine tuned improvements to the nonplanar wingtip design so as to minimize the C_{Dpar} penalty while maintaining the reduction in C_{Di}.

4. Conclusion and future work

Lift and drag data was experimentally obtained for a proposed wingtip device employing wingtip gaps as shown in figure 1. The wingtip gaps, γ, are defined as the total gap size as a percentage of the wing's chord. Results show that, for a planar wing with $\gamma = 20\%$, the mean C_L over the pre-stall region increased by 7.25%, and C_{Lmax} increased by 5.60% as compared to a wing without wingtip gaps, where $\gamma = 0\%$. The nonplanar configuration also shows an improvement of C_L and C_{Lmax} when the wingtip gaps were deployed to $\gamma = 20\%$.

The nonplanar wingtip devices reduced the induced drag of the wing, however, this came at a cost of increased parasitic drag. With a different design of nonplanar wingtip devices, the induced drag could be reduced without incurring a significant parasitic drag penalty, thus making the nonplanar design viable. The nonplanar design may not be viable under all conditions, but instead, by adapting wingtip geometry, the wing-winglet system could be morphed to improve performance and increase mission adaptability.

The experiment show that planar wingtip gaps were sensitive to wingtip angles of attack relative to the base wing angle of attack, α_t, whereas the nonplanar configuration was not. The effects of varying γ were shown to not be strongly related to the planarity of the wingtip device. In essence, the wingtip gap effects can be decoupled from the planarity effects in the design of similar wingtip device, where wingtip gaps had a favorable effect on lift while wing non-planarity has a favorable effect on induced drag. Decoupling these two effects will allow designers to take advantage of the properties of both parameters.

Future work includes optimizing the design of the nonplanar winglets to minimize the parasitic drag penalty and maximize the reduction in induced drag. The effects of wingtip angles of attack can be studied numerically to determine optimum α_t for a given operating condition. Work can also be done on creating an adaptive wingtip design that could dynamically vary γ, α_t, and the geometry of the wingtip device to improve performance under a wide variety of flight conditions. Moreover, these adaptive wingtip devices can be used for yaw stability and aircraft control, as suggested by [24] and [25], respectively.

Acknowledgments

The authors would like to acknowledge and thank the Mechanical Science and Engineering Department at the University of Illinois Urbana-Champaign for continued support and resources. The authors would also like to thank the Renewable Energy & Turbulent Environment Group for the use of their facilities.

ORCID iDs

Aimy Wissa https://orcid.org/0000-0002-8468-511X

References

[1] Tobalske B W 2000 Biomechanics and physiology of gait selection in flying birds *Physiol. Biochem. Zool.* **73** 736–50
[2] Mohamed A, Massey K, Watkins S and Clothier R 2014 The attitude control of fixed-wing mavs in turbulent environments *Prog. Aerosp. Sci.* **66** 37–48
[3] Miley S 1974 On the design of airfoils for low reynolds numbers *2nd Int. Symp. on the Technology and Science of Low Speed and Motorless Flight* p 1017
[4] Withers P C 1981 An aerodynamic analysis of bird wings as fixed aerofoils *J. Exp. Biol.* **90** 143–62

[5] Carruthers A, Walker S, Thomas A and Taylor G 2010 Aerodynamics of aerofoil sections measured on a free-flying bird *Proc. Inst. Mech. Eng. G* **224** 855–64
[6] Taylor G K, Carruthers A C, Hubel T Y and Walker S M 2012 Wing morphing in insects, birds and bats: mechanism and function *Morphing Aerospace Vehicles and Structures* (New York: Wiley) pp 11–40
[7] Tucker V A 1995 Drag reduction by wing tip slots in a gliding harris' hawk, parabuteo unicinctus *J. Exp. Biol.* **198** 775–81
[8] Savile D 1957 Adaptive evolution in the Avian wing *Evolution* **11** 212–22
[9] Shyamal L 2015 Counteracting extremes enabling normal flying: insights for global governance from birds on the wing and the dodo (available at: www.laetusinpraesens.org/docs10s/flying.php)
[10] Watkins S, Milbank J, Loxton B J and Melbourne W H 2006 Atmospheric winds and their implications for microair vehicles *AIAA J.* **44** 2591–600
[11] US Fish and Wildlife Service Feather atlas 2010 (available at: www.fws.gov/lab/featheratlas/)
[12] Kroo I 2001 Drag due to lift: concepts for prediction and reduction *Ann. Rev. Fluid Mech.* **33** 587–617
[13] Whitcomb R T 1976 A design approach and selected wind tunnel results at high subsonic speeds for wing-tip mounted winglets *Technical Report: NASA-TN-D-8260, L-10908* (Washington, DC: NASA)
[14] Kroo I 2005 Nonplanar wing concepts for increased aircraft efficiency *Innovative Configurations and Advanced Concepts for Future Civil Aircraft* (Flanders: von Karman Institute for Fluid Dynamics Lecture Series) pp 6–10
[15] La Roche U and Palffy S 1996 Wing-grid a novel device for reduction of induced drag on wings *ICAS Proc.* **20** 2303–9
[16] Fluck M and Crawford C 2014 A lifting line model to investigate the influence of tip feathers on wing performance *Bioinspir. Biomim.* **9** 046017
[17] Cerón-Muñoz H D and Catalano F M 2006 Experimental analysis of the aerodynamic characteristics adaptive of multi-winglets *Proc. Inst. Mech. Eng. G* **220** 209–15
[18] Guerrero J E, Maestro D and Bottaro A 2012 Biomimetic spiroid winglets for lift and drag control *C. R. Mec.* **340** 67–80
[19] Smith M, Komerath N, Ames R, Wong O and Pearson J 2001 Performance analysis of a wing with multiple winglets *19th AIAA Applied Aerodynamics Conf.* p 2407
[20] Selig M S 1995 *Summary of Low Speed Airfoil Data* vol 1 (Virginia Beach, VA: SoarTech)
[21] Graham R R 1932 Safety devices in wings of birds *J. R. Aeronaut. Soc.* **36** 24–58
[22] McCormick B W 1995 *Aerodynamics, Aeronautics, and Flight Mechanics* vol **2** (New York: Wiley)
[23] Niţă M and Scholz D 2012 Estimating the oswald factor from basic aircraft geometrical parameters *Deutsche Gesellschaft für Luft- und Raumfahrt–Lilienthal–Oberth e.V., Bonn*
[24] Sachs G and Moelyadi M A 2006 Effect of slotted wing tips on yawing moment characteristics *J. Theor. Biol.* **239** 93–100
[25] Bourdin P, Gatto A and Friswell M 2008 Aircraft control via variable cant-angle winglets *J. Aircr.* **45** 414–23